Stem Cell Reports
Article
ISSCR
OPEN ACCESS

Cellular and electrophysiological characterization of triadin knockout syndrome using induced pluripotent stem cell-derived cardiomyocytes

Daniel J. Clemens,[1] Dan Ye,[1,2] Lili Wang,[3] C.S. John Kim,[1,2] Wei Zhou,[1,2] Steven M. Dotzler,[1] David J. Tester,[1,2] Isabelle Marty,[4] Bjorn C. Knollmann,[3,5] and Michael J. Ackerman[1,2,6,7,*]

[1]Department of Molecular Pharmacology & Experimental Therapeutics, Windland Smith Rice Sudden Death Genomics Laboratory, Mayo Clinic, Rochester, MN, USA
[2]Department of Cardiovascular Medicine, Division of Heart Rhythm Services, Mayo Clinic, Rochester, MN, USA
[3]Department of Medicine, Vanderbilt Center for Arrhythmia Research and Therapeutics, Nashville, TN, USA
[4]University Grenoble Alpes, INSERM U1216, CHU Grenoble Alpes, Grenoble Institute Neurosciences, 38000 Grenoble, France
[5]Vanderbilt School of Medicine, Nashville, TN, USA
[6]Department of Pediatric and Adolescent Medicine, Division of Pediatric Cardiology, Mayo Clinic, Rochester, MN, USA
[7]Twitter: @MJAckermanMDPhD
*Correspondence: ackerman.michael@mayo.edu
https://doi.org/10.1016/j.stemcr.2023.04.005

SUMMARY

Triadin knockout syndrome (TKOS) is a malignant arrhythmia disorder caused by recessive null variants in *TRDN*-encoded cardiac triadin. Induced pluripotent stem cell-derived cardiomyocytes (iPSC-CMs) were generated from two unrelated TKOS patients and an unrelated control. CRISPR-Cas9 gene editing was used to insert homozygous TRDN-p.D18fs*13 into a control line to generate a TKOS model ($TRDN^{-/-}$). Western blot confirmed total knockout of triadin in patient-specific and $TRDN^{-/-}$ iPSC-CMs. iPSC-CMs from both patients revealed a prolonged action potential duration (APD) at 90% repolarization, and this was normalized by protein replacement of triadin. APD prolongation was confirmed in $TRDN^{-/-}$ iPSC-CMs. $TRDN^{-/-}$ iPSC-CMs revealed that loss of triadin underlies decreased expression and co-localization of key calcium handling proteins, slow and decreased calcium release from the sarcoplasmic reticulum, and slow inactivation of the L-type calcium channel leading to frequent cellular arrhythmias, including early and delayed afterdepolarizations and APD alternans.

INTRODUCTION

Triadin knockout (TKO) syndrome (TKOS) is a rare, recently discovered genetic heart rhythm disorder caused by recessively inherited homozygous or compound heterozygous null variants in *TRDN*-encoded cardiac triadin 1 (CT1) (Altmann et al., 2015; Clemens et al., 2019, 2020a; Roux-Buisson et al., 2012). TKOS is characterized by a malignant and potentially lethal phenotype. Recently published data from the International Triadin Knockout Syndrome Registry found that 95% of TKOS patients are symptomatic and 81% have experienced at least one sudden cardiac arrest, with the first event occurring at an average age of 3 years (Clemens et al., 2019). In addition, 75% of symptomatic patients have experienced breakthrough cardiac events (BCEs) despite various treatment strategies. Patients with TKOS display features of multiple arrhythmia disorders, including transient QT prolongation, ectopy on stress testing, and extensive T-wave inversions in the precordial leads (Clemens et al., 2019). Interestingly, some patients exhibit skeletal myopathy or slight proximal weakness because of loss of triadin in skeletal muscle (Clemens et al., 2019; Engel et al., 2017; Roux-Buisson et al., 2012).

Triadin is a critical protein within the cardiac calcium release unit (CRU) complex where the L-type calcium channel (LTCC) is juxtaposed to the *RYR2*-encoded ryanodine receptor 2/calcium release channel (RYR2) on the junctional sarcoplasmic reticulum (jSR) (Guo et al., 1996; Knollmann, 2009). This multi-protein complex is responsible for mediating calcium sensing and proper excitation-contraction coupling in the heart. Triadin binds to multiple proteins within the CRU, including RYR2, calsequestrin 2 (CASQ2), and junctin, and has multiple functions, including mediating proper calcium release from the jSR through RYR2, as well as stabilization of the CRU structure (Chopra and Knollmann, 2013; Knollmann, 2009).

Ablation of triadin causes multiple structural and functional cardiac abnormalities in mice (Cacheux et al., 2020; Chopra et al., 2009). However, although these knockout mice studies have yielded many insights into the consequences of loss of triadin, this has not yet been investigated in humans. Although TKO mice do exhibit ventricular arrhythmias, loss of triadin is not lethal in mice (Cacheux et al., 2020; Chopra et al., 2009). Humans, in contrast, exhibit a potentially highly lethal phenotype of sudden cardiac arrest and sudden cardiac death in early childhood. Therefore, in this study, we utilized human induced pluripotent stem cell-derived cardiomyocytes (CMs; iPSC-CMs) to examine the cellular and electrophysiological phenotype of TKOS in humans.

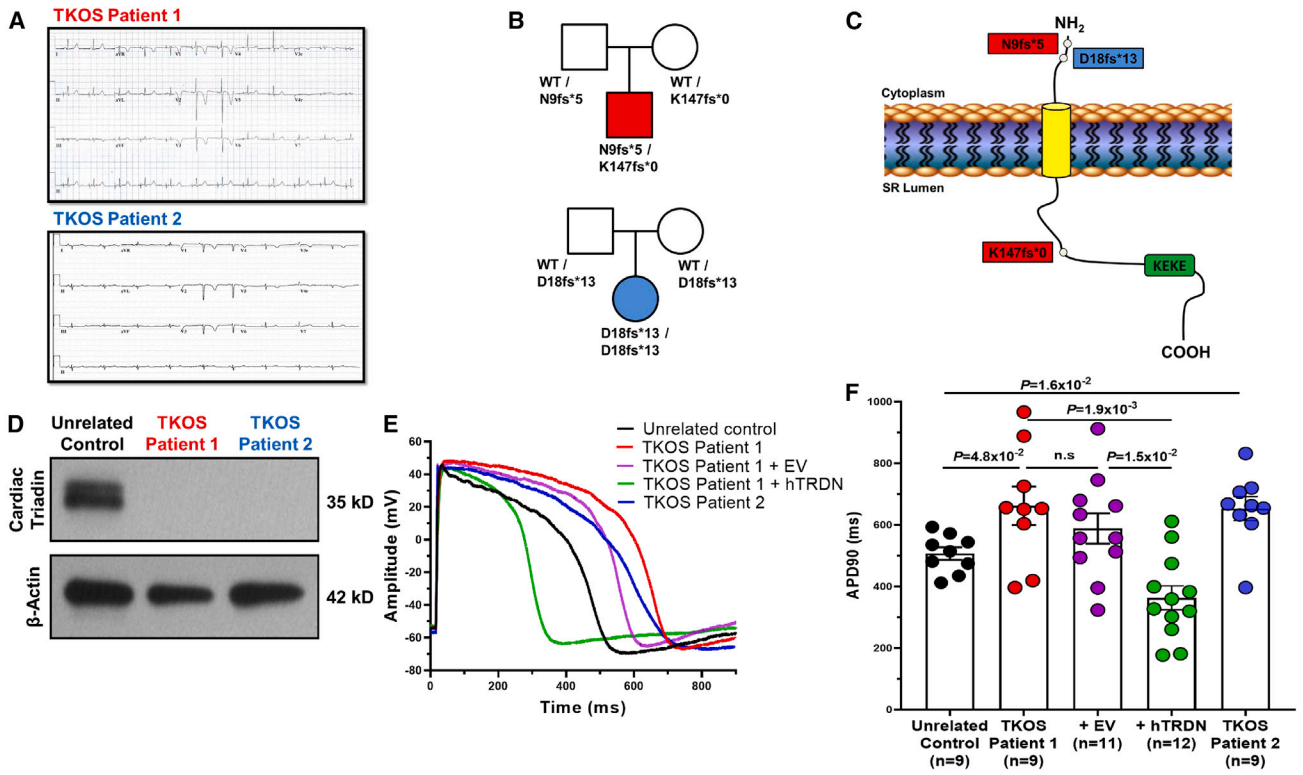

Figure 1. Phenotype of patients with triadin knockout syndrome (TKOS) and TKOS patient-derived induced pluripotent stem cell-derived cardiomyocytes (iPSC-CMs)

(A) Representative 12-lead electrocardiograms from TKOS patients 1 and 2 showing QT prolongation and T-wave inversions in precordial leads V1–V3.

(B) Family pedigrees for TKOS patients 1 (red) and 2 (blue). Circles denote female, and squares denote male.

(C) Protein topology map of *TRDN*-encoded cardiac triadin 1. Each white dot represents the location of a corresponding pathogenic variant. The KEKE domain is the region known to be responsible for the interaction and binding of both CASQ2 and RYR2 (amino acids 210–224).

(D) Western blot detecting cardiac triadin 1 in unrelated control (lane 1) and patient-derived (lanes 2–3) iPSC-CMs.

(E and F) Representative action potential tracings and (F) action potential duration at 90% repolarization (APD90) in iPSC-CMs derived from unrelated control (one differentiation), TKOS patient 1 (one differentiation), TKOS patient 1 transfected with either empty vector (EV; one differentiation) or human cardiac triadin 1 cDNA-containing plasmid (hTRDN; one differentiation), and TKOS patient 2 (one differentiation). Graphs are presented as mean ± SEM. Kruskal-Wallis tests with post hoc Dunn's multiple comparisons tests were conducted to determine significance.

RESULTS

Loss of triadin leads to action potential prolongation in patient-specific TKOS iPSC-CMs

We generated iPSCs from two unrelated patients with TKOS along with a previously characterized unrelated control (Figures 1A–1C) (Estes et al., 2019). Detailed clinical and genetic information for both patients can be found in the supplemental information. iPSCs generated from the patients expressed relevant pluripotent markers and have a normal karyotype (Figure S1). All variants were confirmed by Sanger sequencing (Figure S2).

iPSCs from both patients and the unrelated control were differentiated into CMs to create iPSC-CMs using a previously established protocol (Burridge et al., 2014). iPSC-CMs from all three lines expressed multiple cardiac maturity markers (Figure S3). To measure the expression of triadin in these lines, we performed a western blot using an antibody specific to the cardiac isoform of triadin (CT1) (Roux-Buisson et al., 2012). Although the unrelated control displayed a double band at ~35 kDa representing the glycosylated and unglycosylated forms of CT, there was no detectable triadin in iPSC-CMs from either patient, confirming that these TKOS patients are indeed triadin null (Figure 1D).

To assess the electrophysiological phenotype of TKOS, we performed action potential (AP) measurements on single iPSC-CMs paced at 1 Hz (Figure 1E). Although there were no changes in either resting membrane potential (RMP) or AP amplitude, the AP duration (APD) at 90% repolarization

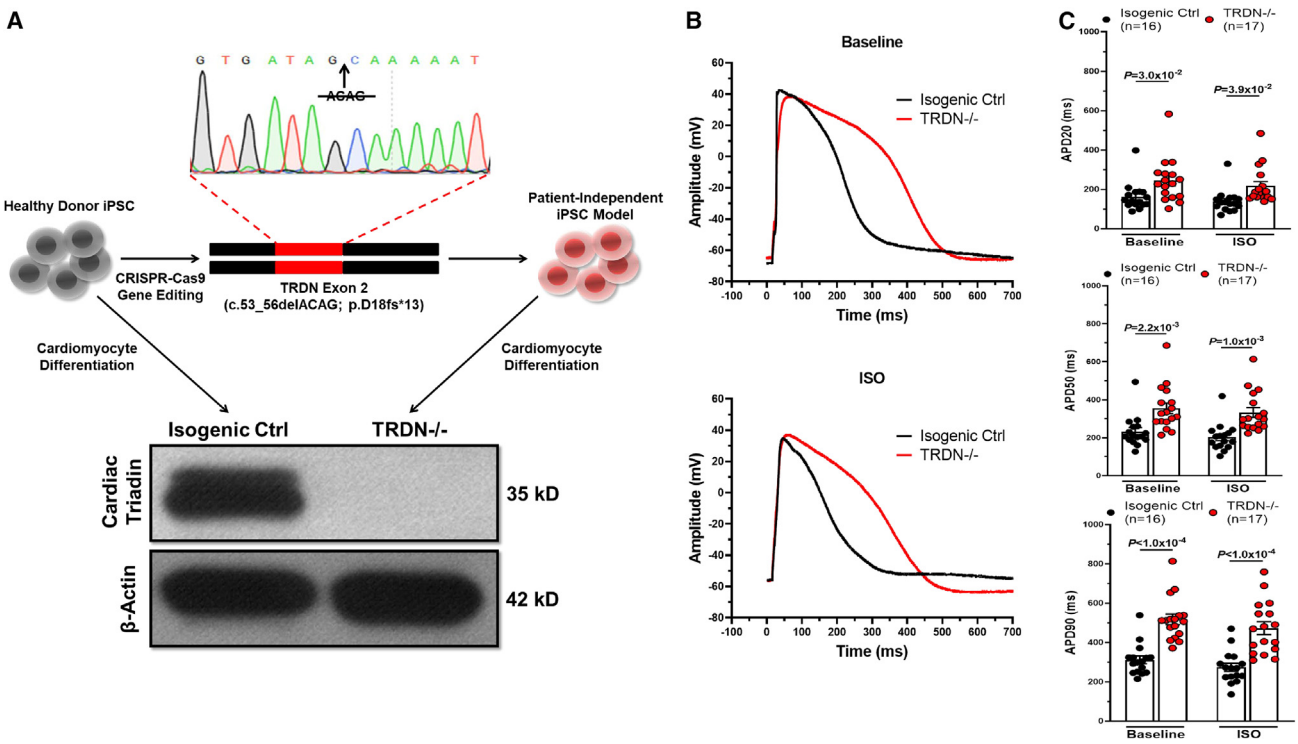

Figure 2. Generation of a variant-inserted TRDN$^{-/-}$ iPSC-CM model of TKOS

(A) A schematic showing the insertion of a homozygous c.53_56delACAG variant (p. D18fs*13) into a healthy donor iPSC line using CRISPR-Cas9 and western blot detecting cardiac triadin 1 in isogenic control (lane 1) and in TRDN$^{-/-}$ iPSC-CMs (lane 2).

(B and C) Representative action potential traces and (C) action potential duration at 20% (APD20), 50% (APD50), and 90% (APD90) repolarization at baseline and after treatment with 1 μM isoproterenol (ISO) in isogenic control (two differentiations) and TRDN$^{-/-}$ (four differentiations) iPSC-CMs.

Graphs are presented as mean ± SEM. Two-way ANOVAs were conducted to determine significance. Ctrl, control.

(APD90) was prolonged significantly in TKOS patients 1 and 2 compared with unrelated control (Figure 1F; Table S1).

Protein Replacement of Triadin Corrects AP Prolongation in Patient-Specific TKOS iPSC-CMs

Because patients with TKOS are natural knockouts for triadin, we hypothesized that protein replacement by delivery of the wild-type CT1 isoform (Ensembl: ENST00000546248) could correct the APD prolongation observed in our patient-specific TKOS iPSC-CMs. To test this, we transfected iPSC-CMs derived from TKOS patient 1 with either an empty vector or human CT1 cDNA-containing plasmid (hTRDN) tagged with GFP (Figure S4A). We then performed AP measurements on single GFP-expressing iPSC-CMs (Figures 1E and S4B). TKOS patient 1-derived iPSC-CMs transfected with empty vector did not display a significant change in APD90 compared with untransfected iPSC-CMs. However, hTRDN-transfected TKOS patient 1-derived iPSC-CMs showed a significantly shorter APD90 than both untransfected and EV-transfected iPSC-CMs (Figure 1F; Table S2). These results indicate protein replacement of triadin can correct the abnormal APD phenotype in patient-specific iPSC-CMs and could serve as a potential treatment for patients with TKOS. Interestingly, overexpression of hTRDN in TKOS patient 1-derived iPSC-CMs elevated the RMP by more than 10 mV (Table S2), indicating it may have additional effects such as a loss-of-function effect on the I_{K1} channel.

Loss of triadin leads to AP prolongation and cellular arrhythmias in TRDN$^{-/-}$ iPSC-CMs

Following the discovery of a disease phenotype in our TKOS patient-specific iPSC-CMs, we developed a variant-inserted iPSC-CM model of TKOS to better characterize the mechanism by which loss of triadin leads to the severe arrhythmic phenotype observed in patients with TKOS. To do this, we utilized CRISPR/Cas9 to introduce a homozygous TRDN-p.D18fs*13 (c.53_56delACAG) variant, which is the same variant observed in TKOS patient 2, into a well-characterized control iPSC line generated from a healthy donor (Figure 2A) (Ran et al., 2013; Wang et al., 2018). Throughout the remainder of this investigation, we utilized the healthy

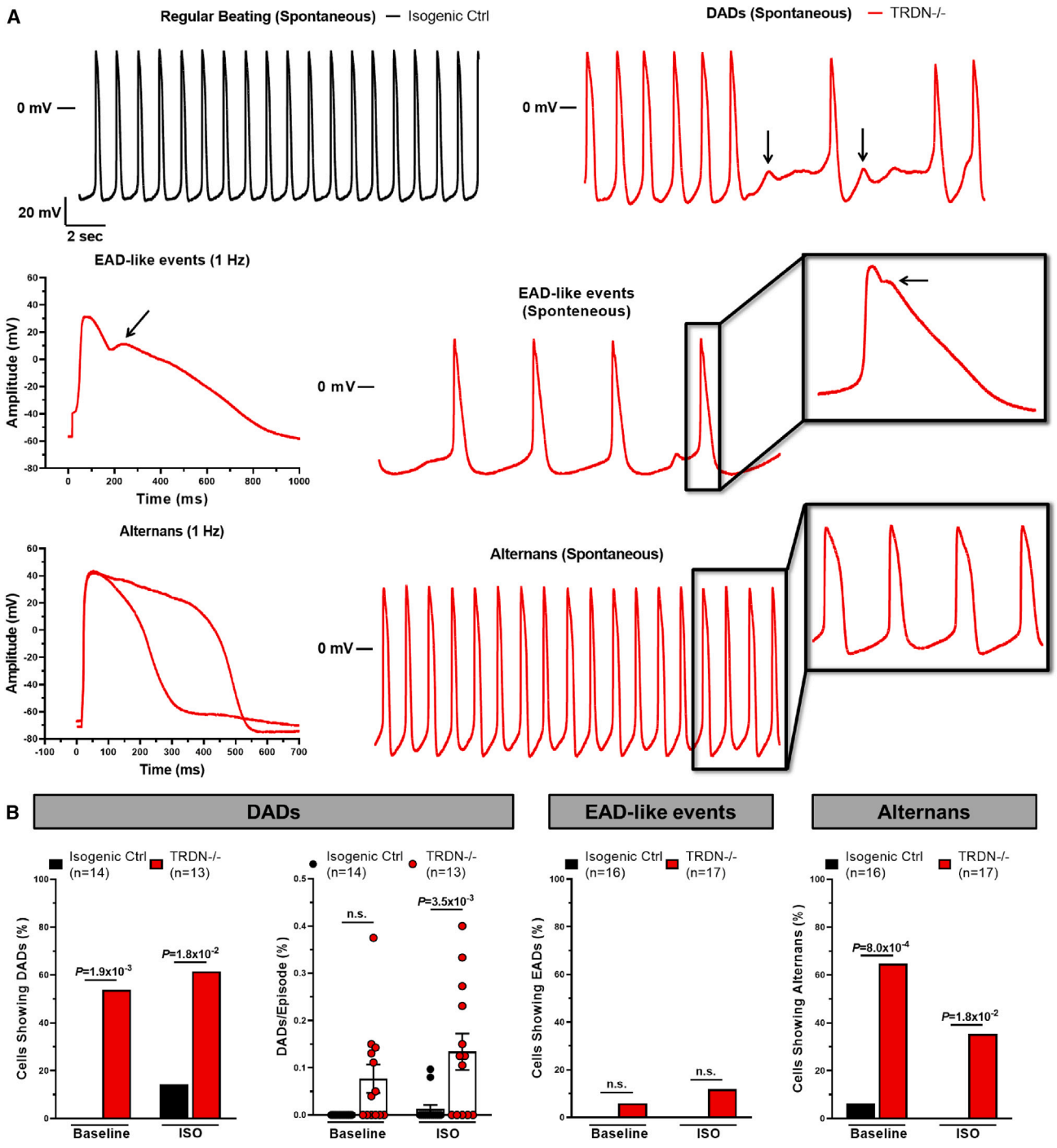

Figure 3. TRDN$^{-/-}$ iPSC-CMs display cellular arrhythmias

(A) Representative action potential traces derived from isogenic control (black) and TRDN$^{-/-}$ (red) iPSC-CMs recording during 1-Hz pacing or spontaneous beating. Black arrows indicate individual delayed afterdepolarizations (DADs) or early afterdepolarization (EAD)-like events. Black boxes contain zoomed-in representative action potential traces.

(B) The two left panels depict the number of cells showing DADs from either paced at 1 Hz or spontaneous action potential (gap-free) measurements and the number of DADs per action potential (DADs/episode) from spontaneous action potential measurements only in isogenic control (two differentiations) and TRDN$^{-/-}$ (four differentiations) iPSC-CMs at baseline and after treatment with 1 μM ISO. Fischer's exact tests were used to determine significance between two groups (first panel). Two-way ANOVAs with Tukey's multiple

(legend continued on next page)

donor iPSCs as an isogenic control and two independent clones of the variant-inserted TKOS iPSCs referred to as TRDN$^{-/-}$. Both clones of TRDN$^{-/-}$ expressed relevant markers of pluripotency and had a normal karyotype (Figure S1). Sanger sequencing confirmed the presence of the homozygous p. D18fs*13 variant (Figure S2).

To study the mechanism of TKOS in humans, we differentiated isogenic control and TRDN$^{-/-}$ iPSCs into CMs (Figure S3). Western blot with a CT antibody confirmed the absence of triadin in TRDN$^{-/-}$ iPSC-CMs (Figure 2A). At baseline, TRDN$^{-/-}$ iPSC-CMs displayed a significantly prolonged APD at 20% and 50% (APD20 and APD50) repolarization and APD90 (Figures 2B and 2C; Table S3).

Because many patients with TKOS have experienced cardiac events during exertion, we also tested the effects of isoproterenol (ISO) in our iPSC-CMs (Figure 2B). Following treatment with 1 μM ISO, both APD50 and APD90 remained prolonged in TRDN$^{-/-}$ iPSC-CMs compared with isogenic control (Figure 2C; Table S3).

We also observed multiple unique cellular arrhythmias in TRDN$^{-/-}$ iPSC-CMs both when paced at 1 Hz and during spontaneous beating. These included delayed afterdepolarizations (DADs), early afterdepolarization (EAD)-like events, and APD alternans (Figure 3A). DADs were not observed while CMs were being paced but were significantly more common in TRDN$^{-/-}$ iPSC-CMs than isogenic control during measurements of spontaneous beating at baseline and following treatment with ISO (Figure 3B). We also assessed the rate at which DADs occur by measuring the number of DADs per AP (DADs/episode), and this rate was significantly higher in TRDN$^{-/-}$ iPSC-CMs compared with isogenic control after ISO (Figure 3B). Unique EAD-like events were observed only in TRDN$^{-/-}$ iPSC-CMs and not in isogenic control iPSC-CMs, but they did not reach statistical significance at baseline or after ISO (Figures 3A and 3B). APD alternans was the most common arrhythmia in TRDN$^{-/-}$ iPSC-CMs at baseline (Figures 3A and 3B). Interestingly, alternans was observed less often following treatment with ISO but was still significantly more common in TRDN$^{-/-}$ iPSC-CMs (Figure 3B). These results indicate that loss of triadin confers increased susceptibility for not only APD prolongation but also significant cellular arrhythmias.

Loss of triadin leads to slow inactivation of $Ca_V1.2$ in TRDN$^{-/-}$ iPSC-CMs

Based on previous studies in murine TKOS, we hypothesized that the most likely cause of APD prolongation in TRDN$^{-/-}$ iPSC-CMs was slow inactivation of the cardiac LTCC ($Ca_V1.2$) due to a decrease in calcium-dependent inactivation (CDI). To test this hypothesis, we performed $Ca_V1.2$ current measurements using standard voltage-clamp protocols (Figure S5A). Peak current density was slightly decreased in TRDN$^{-/-}$ iPSC-CMs but did not reach statistical significance (Figure S5B; Table S4). $V_{1/2}$ of both activation and inactivation showed a minor right-shift toward more positive voltages in TRDN$^{-/-}$, but slope factor showed no change (Figure S5C; Table S4). Interestingly, fast inactivation τ was significantly slower in TRDN$^{-/-}$ iPSC-CMs compared with isogenic control at 30 mV (Figures S5D and S5E), but there were no changes in slow inactivation τ (Figure S5F), amplitude of fast and slow inactivation (Figure S6A), or normalized $Ca_V1.2$ persistent current (Figure S5G; Table S4).

To better evaluate the effects of CDI on LTCC currents, we performed a second set of $Ca_V1.2$ measurements using a pipette solution with a low concentration of EGTA to increase calcium-dependent coupling between $Ca_V1.2$ and RYR2 (Figure 4A). These measurements revealed an insignificant decrease in peak current, only a minimal depolarized shift in $V_{1/2}$ of activation, and no changes in slope factor for activation or inactivation between isogenic control and TRDN$^{-/-}$ iPSC-CMs (Figures 4B and 4C; Table S4). Fast inactivation τ of TRDN$^{-/-}$ iPSC-CMs was significantly slower at 20 mV (Figures 4D and 4E), whereas slow inactivation τ (Figure 4F) and amplitude of both fast and slow inactivation (Figure S6B) remained unchanged. Notably, under these conditions, the TRDN$^{-/-}$ normalized persistent current was much greater than in isogenic control (Figure 4G; Table S4).

To confirm that impaired CDI was the underlying cause of the altered $Ca_V1.2$ kinetics, we performed a third set of $Ca_V1.2$ measurements in which we replaced Ca^{2+} with Ba^{2+} in the bath solution (in addition to using low EGTA pipette solution; Figure 5A). This prevents calcium-induced calcium release from the jSR and eliminates CDI of $Ca_V1.2$. When we did this, we found that there were no differences in fast or slow inactivation τ at 0 mV (Figures 5B–5D) or normalized persistent current in TRDN$^{-/-}$ iPSC-CMs compared with isogenic control (Figure 5E). These results suggest that slow $Ca_V1.2$ inactivation and increased persistent current resulting from decreased CDI are likely the cellular mechanism for the observed APD prolongation in TRDN$^{-/-}$ iPSC-CMs.

Loss of triadin leads to impaired calcium release in TRDN$^{-/-}$ iPSC-CMs

To uncover the cause of decreased $Ca_V1.2$ CDI, we performed Fluo-4 calcium imaging in both isogenic control

comparisons tests were used to determine statistical significance for more than three groups (second panel). The two right panels depict the number of cells showing either EAD-like events or alternans from either paced at 1 Hz or spontaneous action potential measurements in isogenic control (two differentiations) and TRDN$^{-/-}$ (four differentiations) iPSC-CMs at baseline and after treatment with ISO. Fischer's exact tests were used to determine significance between two groups.

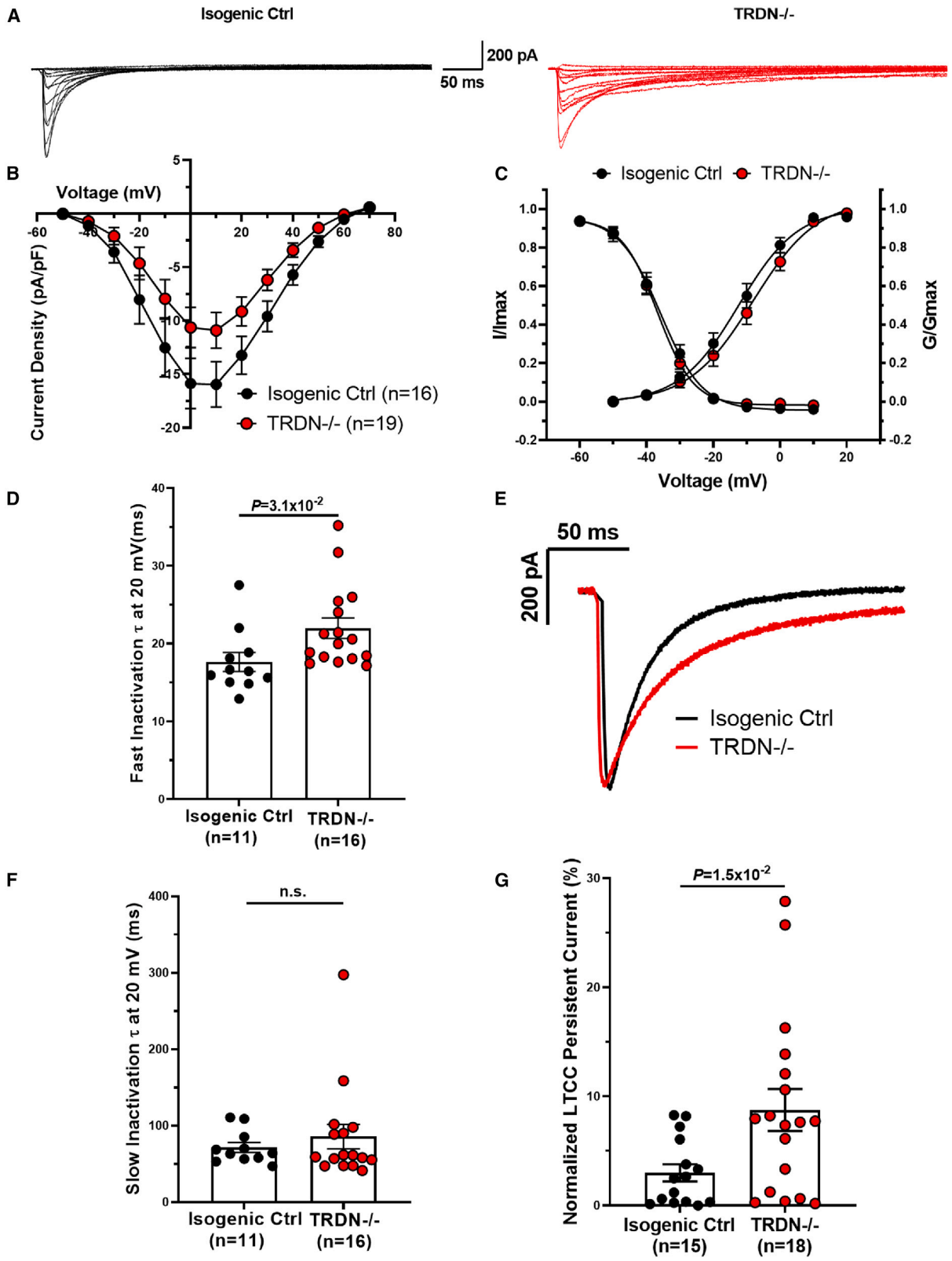

(legend on next page)

and TRDN$^{-/-}$ iPSC-CMs (Figure 6A). At baseline, both calcium transient duration (CTD) at 50% (CTD50) and 90% (CTD90) decay were prolonged significantly in TRDN$^{-/-}$ iPSC-CMs (Figure 6B; Table S5). Calcium transient decay time at both 50% and 90% decay were unchanged and therefore did not contribute to CTD prolongation (Figure 6C; Table S5). However, upstroke time of the calcium transient in TRDN$^{-/-}$ was increased significantly compared with isogenic control, and upstroke velocity was significantly slower (Figure 6D; Table S5). The slow upstroke kinetics in TRDN$^{-/-}$ iPSC-CMs therefore accounts for the observed CTD prolongation, as can be clearly seen from the representative traces in Figure 6A. In addition, the calcium transient amplitude was significantly decreased in TRDN$^{-/-}$ iPSC-CMs compared with isogenic control (Figure 6E; Table S5). We also performed calcium imaging measurements in the setting of β-adrenergic stimulation using ISO and found that all changes in calcium transient kinetics remained consistent following β-adrenergic stimulation (Figures 6A–6E; Table S5). These results suggest that jSR calcium release through RYR2 is impaired and may contribute to a decrease in $Ca_V1.2$ CDI, whereas calcium reuptake through SERCA2A remains unchanged.

Loss of triadin leads to decreased expression and co-localization of key calcium handling proteins in TRDN$^{-/-}$ iPSC-CMs

We next utilized immunofluorescence imaging of multiple calcium handling proteins to determine the causes of slow and decreased calcium release observed in our calcium imaging experiments. Staining of RYR2 and CASQ2, triadin's main interaction partners, revealed a significant decrease in fluorescence of both proteins in TRDN$^{-/-}$ iPSC-CMs (Figure 7A). CASQ2 fluorescence was decreased by over 75%, and RYR2 fluorescence was decreased by ~45% compared with isogenic control (Figure 7A). To confirm these results, we ran western blots and found CASQ2 expression was again decreased by ~75% (Figure 7B). However, RYR2 expression was unchanged, which might be because of lack of good antibodies or the limitations, such as phenotypic heterogeneity, inefficient recapitulation, and genetic instability (Figure 7C).

We also measured the fluorescence intensity of both $Ca_V1.2$ and SERCA2A. Fluorescence of both proteins was unchanged in TRDN$^{-/-}$ iPSC-CMs (Figures S7A and S7B), and these results were confirmed by western blot (Figures S7C and S7D).

Finally, co-localization of RYR2 and CASQ2, which could be visualized as yellow fluorescence in many isogenic control iPSC-CMs, was completely absent in TRDN$^{-/-}$ iPSC-CMs (Figure 7D). The subsequent quantification of Pearson's coefficient of RYR2 and CASQ2 in isogenic control (0.6 ± 0.03, n = 12) or TRDN$^{-/-}$ iPSC-CMs (0.42 ± 0.02, n = 18) indicated that the loss of CASQ2 expression and its co-localization to RYR2 may play a role in impaired calcium release, and none of the changes in calcium handling and $Ca_V1.2$ currents are caused by changes in $Ca_V1.2$ or SERCA2A expression.

DISCUSSION

Since 2012, multiple studies have been published showing null variants in *TRDN* to the cause of a rare recessive arrhythmogenic disease now known as TKOS (Altmann et al., 2015; Broendberg et al., 2017; Clemens et al., 2019, 2020b; O'Callaghan et al., 2018; Rooryck et al., 2015; Rossi et al., 2019; Roux-Buisson et al., 2012; Walsh et al., 2016). Interestingly, prior to the discovery of TKOS in humans, multiple studies were conducted in TKO mice to determine the effects of the loss of triadin in both cardiac and skeletal muscle (Cacheux et al., 2020; Chopra et al., 2009; Oddoux et al., 2009). When studying the cardiac cellular phenotype of TKO mice, a reduction in key proteins of the CRU and altered structure of the jSR were observed. These structural changes led to slow and decreased SR calcium release and loss of the negative feedback loop on the LTCC, resulting

Figure 4. TRDN$^{-/-}$ iPSC-CMs display slow $Ca_V1.2$ inactivation and increased persistent current at low EGTA conditions

(A) Whole-cell $Ca_V1.2$ representative traces from isogenic control and TRDN$^{-/-}$ iPSC-CMs determined from a holding potential of −90 mV to testing potential of +70 mV in 10-mV increments with 500-ms duration.

(B and C) $Ca_V1.2$ current-voltage relationship and (C) $Ca_V1.2$ inactivation-activation curves in isogenic control (three differentiations) and TRDN$^{-/-}$ (three differentiations) iPSC-CMs. Steady-state inactivation was determined from a holding potential of −90 mV to prepulse of 20 mV in 10-mV increments with 5-s duration followed by a test pulse of 30 mV with 500-ms duration.

(D) Inactivation time constants (τ) for the fast phase of $Ca_V1.2$ decay time in isogenic control (three differentiations) and TRDN$^{-/-}$ (three differentiations) iPSC-CMs at 20 mV. Time constants were determined by fitting a biexponential function to current decay.

(E) Representative $Ca_V1.2$ traces at 20 mV showing slow inactivation in TRDN$^{-/-}$ iPSC-CMs compared with isogenic control.

(F) Inactivation time constants (τ) for the slow phase of $Ca_V1.2$ decay time in isogenic control (three differentiations) and TRDN$^{-/-}$ (three differentiations) iPSC-CMs at 20 mV.

(G) Persistent current normalized to peak current at −20 mV shown as percentages for isogenic control (three differentiations) and TRDN$^{-/-}$ (three differentiations) iPSC-CMs.

Graphs are presented mean ± SEM. Unpaired Student's t tests were conducted to determine significance. G/G_{max}, normalized conductance; I/I_{max}, normalized calcium current; ns, not significant.

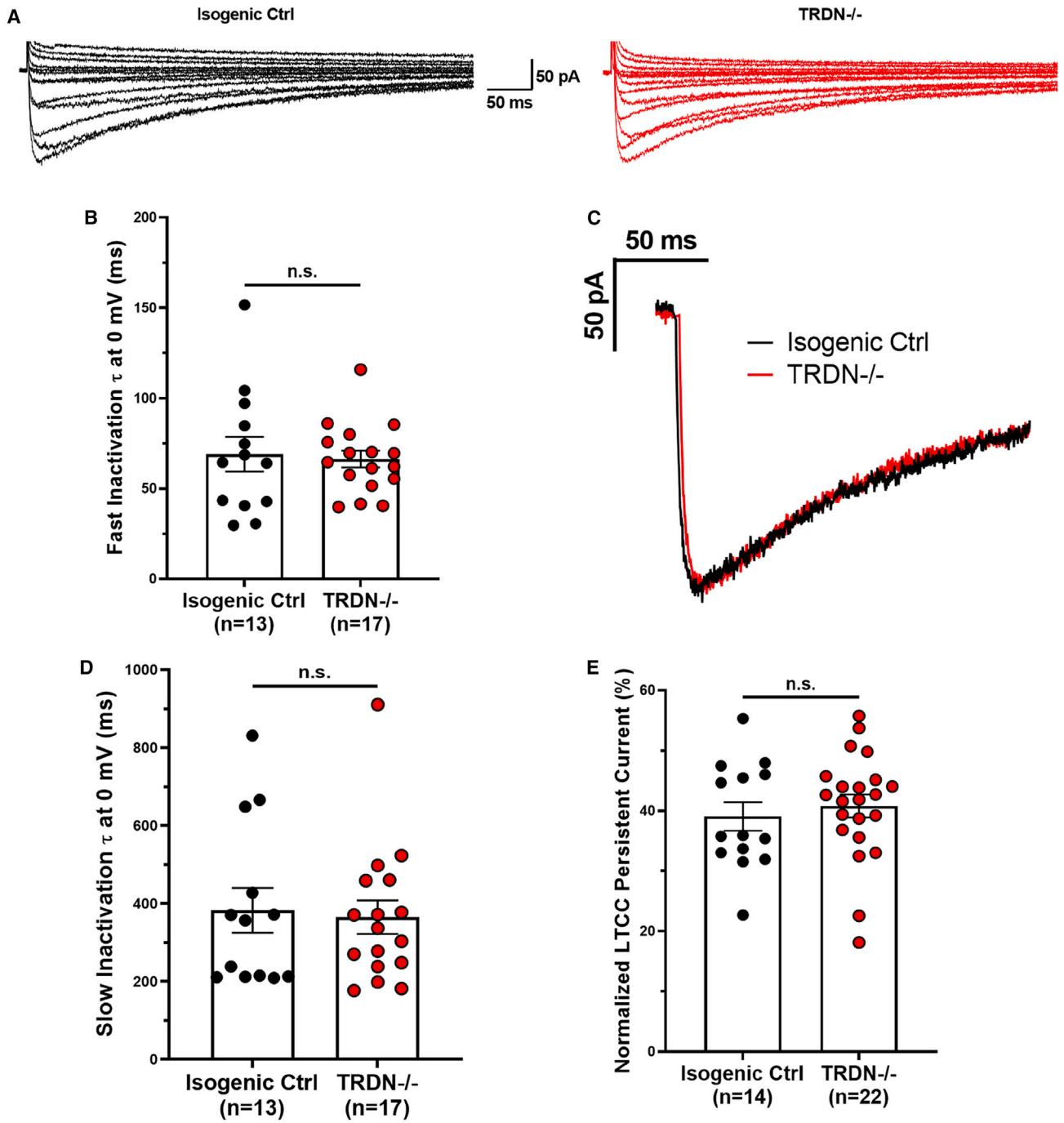

Figure 5. Ba^{2+} replacement eliminates differences in $Ca_V1.2$ inactivation and persistent current at low EGTA conditions in $TRDN^{-/-}$ iPSC-CMs

(A) Whole-cell $Ca_V1.2$ representative traces from isogenic control and $TRDN^{-/-}$ iPSC-CMs determined from a holding potential of −90 mV to testing potential of +70 mV in 10-mV increments with 500-ms duration.

(B) Inactivation time constants (τ) for the fast phase of $Ca_V1.2$ decay time in isogenic control (two differentiations) and $TRDN^{-/-}$ (two differentiations) iPSC-CMs at 0 mV. Time constants were determined by fitting a biexponential function to current decay.

(C) Representative $Ca_V1.2$ traces at 0 mV showing no change in inactivation between isogenic control and $TRDN^{-/-}$ iPSC-CMs.

(legend continued on next page)

in slow inactivation of the LTCC. This in turn led to spontaneous calcium release and ventricular arrhythmias in the setting of β-adrenergic stimulation (Cacheux et al., 2020; Chopra et al., 2009). Although these studies clearly describe the mechanism by which loss of triadin leads to arrhythmia in TKO mice, there are distinct differences between the phenotypes observed in these mice and human patients with TKOS. For this reason, we set out to study the mechanism of disease in humans using patient-specific and patient-independent iPSC-CM models.

In many ways our results are strikingly similar to what has been observed previously in mice. To begin with, as in the TKO mice, loss of triadin in human iPSC-CMs leads to a significant reduction in protein expression of CASQ2. This significant decrease in CASQ2 expression has been observed previously in not only murine cardiac tissue but also skeletal muscle (Cacheux et al., 2020; Chopra et al., 2009), and it is likely caused by an inability of CASQ2 to traffic to the jSR membrane in the absence of triadin (Sleiman et al., 2015). In addition, triadin binds to both RYR2 and CASQ2 and plays a role in mediating their functional interaction (Guo and Campbell, 1995; Kobayashi et al., 2000; Marty, 2015). Therefore, it is not surprising that in TRDN$^{-/-}$ iPSC-CMs we observed a clear loss of co-localization between RYR2 and CASQ2.

Our TRDN$^{-/-}$ iPSC-CMs also displayed significant changes in calcium handling similar to what was observed in mice. Calcium transients in TRDN$^{-/-}$ iPSC-CMs had a slower upstroke and decreased amplitude compared with isogenic control. These results indicate impairment of jSR calcium release through RYR2. The limited ability of RYR2 to interact with CASQ2, along with decreased jSR calcium buffering caused by loss of CASQ2 expression, may serve as an underlying cause of this abnormal calcium release, although future studies will be required to further explore this mechanism. In addition, decay time of calcium transients was unchanged in TRDN$^{-/-}$ iPSC-CMs, indicating that reuptake of calcium into the jSR through SERCA2A is normal, which is consistent with our data showing similar expression of SERCA2A in both isogenic control and TRDN$^{-/-}$ iPSC-CMs.

Also, like the TKO mice, TKOS$^{-/-}$ iPSC-CMs exhibit slow inactivation of the LTCC. Interestingly, when we performed these experiments with a low EGTA pipette solution, thereby increasing coupling between $Ca_V1.2$ and RYR2, TRDN$^{-/-}$ iPSC-CMs also displayed a significantly increased persistent current that was not observed at high EGTA conditions. These results would indicate that the gain of function observed in the LTCC is due to a decrease in CDI, and we confirmed this by showing that Ba^{2+} replacement eliminates changes in LTCC function.

Although there are many similarities between our study and previous studies in mice, our work has uncovered significant new findings. Notably, before a TKOS was discovered in humans, observations from TKO mice prompted speculation that slow inactivation of the LTCC in the absence of triadin could theoretically lead to QT prolongation, and this speculation was satisfied when we later discovered triadin null variants as the root cause for some cases of previously genetically elusive LQTS (Altmann et al., 2015). However, QT prolongation has never been reported in TKO mice. Now, in this study, we have shown for the first time that loss of triadin leads to APD prolongation in a human cardiac cell model. Interestingly, we observed this not only in our variant-inserted TRDN$^{-/-}$ iPSC-CMs but also in two lines of iPSC-CMs derived from unrelated TKOS patients with different disease-causative variants, which suggests that triadin null status, regardless of the causative variants, will render a similar QT-prolonging phenotype in different patients. However, the genomic background of the two unrelated TKOS patient iPSC-CMs and the unrelated control iPSC-CMs differ not only at the TRDN gene locus but will have many differences across their entire genome. Additional genetic differences between the unrelated TKOS patient iPSC-CMs and the unrelated control iPSC-CMs could potentially modify the cellular APD phenotype. When compared with unrelated control, TRDN$^{-/-}$ CMs revealed only APD90 prolongation. Whether additional genetic differences existing between the unrelated control and the TRDN$^{-/-}$ iPSC-CMs resulted in no significant difference in APD20 and APD50 between the two models (unrelated control vs. TRDN$^{-/-}$) is not known. In addition, our data would suggest that slow inactivation and increased persistent current in $Ca_V1.2$ are indeed the underlying cause of QT prolongation in patients with TKOS.

Another key difference between TKO mice and patients with TKOS is the severity of the arrhythmic phenotype. The mice do exhibit ventricular arrhythmias, but only in the setting of β-adrenergic stimulation (Cacheux et al., 2020; Chopra et al., 2009). Patients with TKOS, in contrast, exhibit a severe arrhythmic phenotype that, left untreated, has been fatal in multiple cases (Clemens et al., 2019; Rooryck et al., 2015). In addition, although many cardiac events

(D) Inactivation time constants (τ) for the slow phase of $Ca_V1.2$ decay time in isogenic control (two differentiations) and TRDN$^{-/-}$ (two differentiations) iPSC-CMs at 0 mV.

(E) Persistent current normalized to peak current at −20 mV shown as percentages for isogenic control (two differentiations) and TRDN$^{-/-}$ (two differentiations) iPSC-CMs.

Graphs are presented as mean ± SEM. Unpaired Student's t tests were conducted to determine significance.

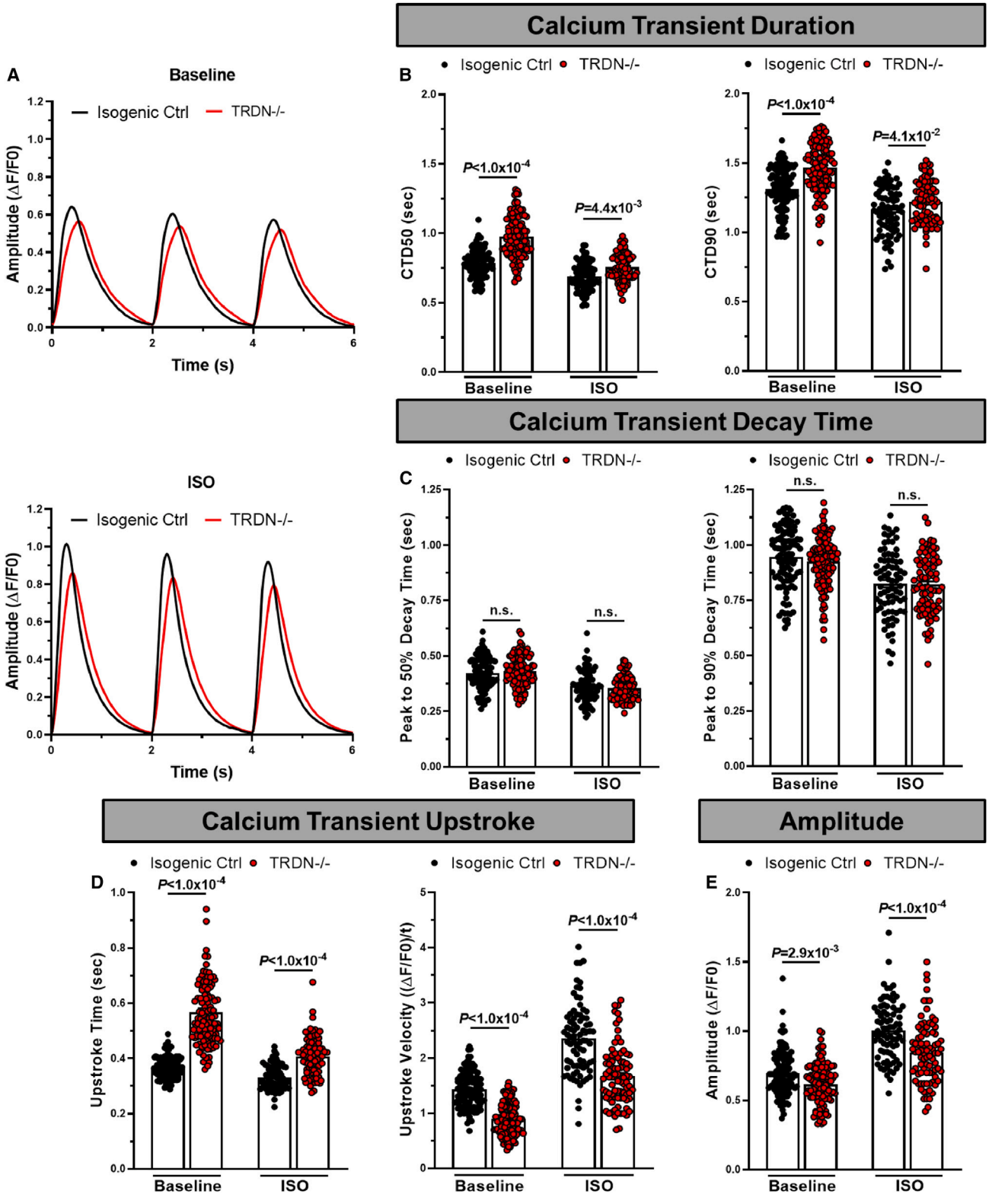

(legend on next page)

experienced by TKOS patients occurred in the setting of β-adrenergic stimulation (physical exertion, fear, etc.), many others had no trigger at all (Clemens et al., 2019). Our data in TRDN$^{-/-}$ iPSC-CMs also suggest a severe arrhythmic phenotype. We observed multiple types of cellular arrhythmia not only after treatment with ISO but also at baseline. This would suggest that β-adrenergic stimulation can serve as an arrhythmic trigger, but unlike in mice, it is not necessary for an arrhythmia to occur.

Besides providing a mechanism by which loss of triadin leads to arrhythmia, our results provide further evidence for TKOS being a unique "crossover" disorder as opposed to either simply LQTS or CPVT. Our TRDN$^{-/-}$ iPSC-CMs displayed significant APD prolongation, as well as EAD-like events and APD alternans, which are common features of LQTS (Itzhaki et al., 2011; Maguy et al., 2020; Schwartz et al., 2020). In addition, we observed jSR calcium mishandling through RYR2 and DADs, which are hallmarks of CPVT (Itzhaki et al., 2012; Schwartz et al., 2020). It is also important to note that a significant decrease in CASQ2 expression, like what we see in TRDN$^{-/-}$ iPSC-CMs, underlies CPVT type 2, and this may also play a role in the arrhythmic phenotype of TKOS (Lahat et al., 2001; Rizzi et al., 2008). These data corroborate what has been observed in patients with TKOS who display clinical features of both LQTS and CPVT, such as QT prolongation and ectopy on stress testing. Therefore, we encourage the continued use of the term TKOS as opposed to either LQT17 or CPVT5, as has been previously suggested.

Interestingly, TKO mice, which display a less malignant phenotype than TKOS patients, do not show a significant QT phenotype and more closely resemble CPVT, whereas TRDN$^{-/-}$ iPSC-CMs have a crossover phenotype of which includes features of both LQTS and CPVT. Therefore, our data would suggest that having features of multiple arrhythmia disorders may serve as an explanation as to why humans seem to exhibit a more malignant phenotype, although further studies will be necessary to confirm this.

One of the features of the severe phenotype of TKOS is its refractory nature to conventional treatment strategies, which highlights the importance of developing novel therapeutics. Because these patients are natural knockouts for triadin, TKOS serves as an ideal candidate for protein replacement treatment using an adeno-associated virus serotype 9-based delivery of the wild-type CT1 isoform (Bongianino and Priori, 2015). Introducing normal CT1 into a TKOS patient's CMs may very well correct their abnormal arrhythmogenic phenotype. In fact, this approach has treated effectively the CPVT phenotype of TKO mice (Cacheux et al., 2020), and we have now shown in this study that protein replacement of triadin can correct the APD prolongation observed in patient-specific TKOS iPSC-CMs, thereby providing preliminary evidence that *TRDN* gene therapy could serve as a more effective treatment strategy for patients with TKOS.

Limitations

Although we have provided substantial evidence that slow inactivation and increased persistent current in $Ca_V1.2$ underlie the significant APD prolongation observed in TRDN$^{-/-}$ iPSC-CMs, we cannot currently rule out the potential contribution of other ion channels, including the $K_V7.1$ and $K_V11.1$ potassium channels, $Na_V1.5$ sodium channel, and Na^+/Ca^{2+} exchanger (NCX).

Even we have shown that the calcium transients in TRDN$^{-/-}$ iPSC-CMs had a slower upstroke and decreased amplitude compared with isogenic control by using non-ratiometric dye Fluo-4, calcium transient amplitude measured as ΔF/F0 was obtained by implying no changes in F0 between groups. This is a limitation of the study, especially in the presence of ISO.

Mouse and human embryonic stem cell-derived CMs (hESC-CMs) are known to exhibit immature $Ca2^+$ dynamics, such as small whole-cell peak amplitude and slower kinetics relative to those of adult. Immature mouse and hESC-CMs display unsynchronized $Ca2^+$ transients because of the absence of t-tubules and gene products crucial for their biogenesis (Deborah et al., 2009). The absence of a proper transverse-axial tubular system in hiPSC-CMs will affect the maturity of the cells as well, which therefore results in the limitation of the disease model in this study. Electrophysiological measurements were carried out at room temperature (RT), not physiological temperature (37°C), which is not able to completely represent the *in vivo* condition resulting in another limitation of the disease model in this study.

Figure 6. TRDN$^{-/-}$ iPSC-CMs display impaired calcium release

(A) Representative Fluo-4 calcium imaging traces derived from isogenic control and TRDN$^{-/-}$ iPSC-CMs at baseline (top) and after treatment with 1 μM ISO (bottom).

(B) Calcium transient duration at 50% (CTD50; left) and 90% (CTD90; right) decay at baseline and after treatment with ISO.

(C) Calcium transient peak to 50% (left) and 90% (right) decay time at baseline and after treatment with ISO.

(D) Calcium transient upstroke time (left) and upstroke velocity (right) at baseline and after treatment with ISO.

(E) Calcium transient amplitude at baseline and after treatment with ISO (baseline: isogenic control, n = 115, two differentiations; TRDN$^{-/-}$, n = 115, four differentiations; ISO: isogenic control, n = 80, two differentiations; TRDN$^{-/-}$, n = 85, four differentiations).

Graphs are presented as mean ± SEM. Two-way ANOVAs were used to determine significance.

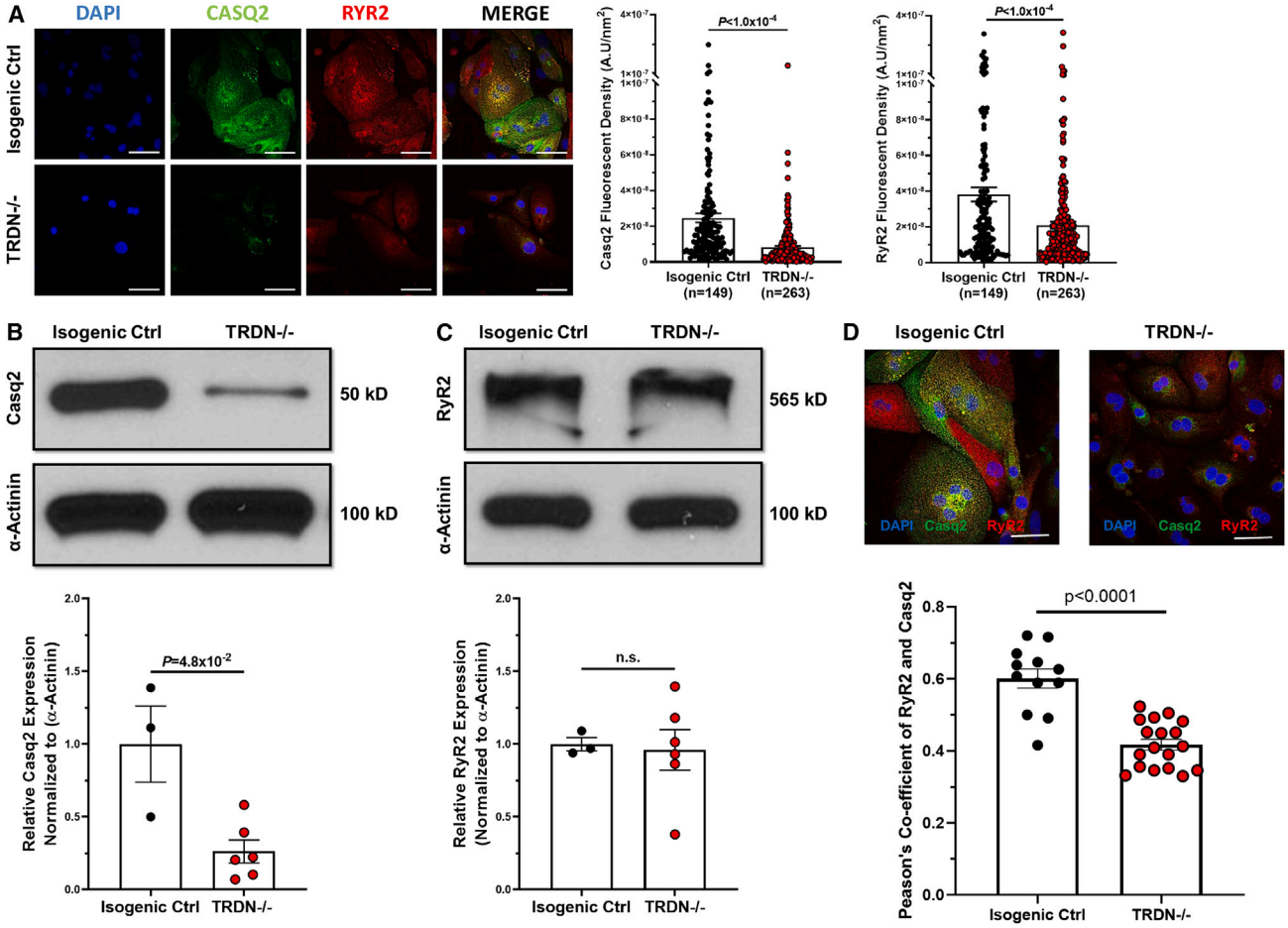

Figure 7. TRDN$^{-/-}$ iPSC-CMs display decreased expression and co-localization of key calcium handling proteins

(A) Representative immunofluorescence images and quantification of RYR2 and CASQ2 protein expression in isogenic control (two differentiations) and TRDN$^{-/-}$ (four differentiations) iPSC-CMs.

(B and C) Western blots detecting CASQ2 and RYR2 and subsequent quantification of relative expression (normalized to α-Actinin) in isogenic control (three differentiations) and TRDN$^{-/-}$ iPSC-CMs (six differentiations).

(D) Representative immunofluorescence images showing co-localization of RYR2 and CASQ2 (yellow) and subsequent quantification of Pearson's coefficient for RYR2 and CASQ2 co-localization in isogenic control or TRDN$^{-/-}$ iPSC-CMs were analyzed using ImageJ with JACoP plug-in. Scale bars, 50 μm.

Graphs represent mean ± SEM. Unpaired Student's t tests (immunofluorescence) or Mann-Whitney tests (western blot) were used to determine significance.

Conclusions

Here, for the first time, we characterize multiple iPSC-CM models of TKOS and provide further evidence for null variants in *TRDN* as a self-sufficient monogenetic substrate for genetic heart disease. These cells display loss of expression and proper localization of key CRU proteins, abnormal calcium handling, slow inactivation of the LTCC, and APD prolongation, which serve as the underlying cause of frequent cellular arrhythmias. These findings suggest a mechanism of disease distinct from either LQTS or CPVT, hence the basis for referring to such patients as having TKOS. In addition, we have provided preliminary evidence that protein replacement gene therapy could serve as a more effective treatment strategy for patients with this malignant and potentially lethal disorder.

EXPERIMENTAL PROCEDURES

Resource availability

Corresponding author

Further information and requests for resources and reagents should be directed to and will be fulfilled by the corresponding author, Michael Ackerman (ackerman.michael@mayo.edu).

Materials availability

All unique/stable reagents generated in this study are available from the corresponding author with a completed Materials Transfer Agreement.

Data and code availability

The data that support the findings of this study are available from the corresponding author on reasonable request.

Samples

Human samples were obtained from patients with TKOS and an unrelated healthy control following written informed consent under Mayo Clinic Institutional Review Board (IRB, 09–006465) study approval. Procedures followed were in accordance with institutional guidelines. Comprehensive methods are available in the supplemental information.

Case descriptions

TKOS patient 1 is a white male who presented initially with fetal bradycardia and subsequently experienced sudden cardiac arrest at 1 year of age. In addition, he had multiple BCEs despite beta blocker treatment. He exhibited a borderline QTc of 475 ms on ECG, along with extensive T-wave inversions in leads V1–V3. Interestingly, this patient also displayed a unique skeletal myopathy caused by the loss of triadin in skeletal muscle. Two compound heterozygous frameshift variants in *TRDN*, p. K147fs*0 and p. N9fs*5, were identified as the basis for his TKOS. TKOS patient 2 is a black female who first experienced cardiac arrest at the age of 1 year. She experienced multiple BCEs despite beta blocker treatment and left cardiac sympathetic denervation. Her ECG showed a prolonged QTc of 500 ms, along with extensive T-wave inversions in precordial leads V1–V4, and she displayed ectopy on stress testing. Whole-exome sequencing revealed a homozygous p.D18fs*13 variant in *TRDN* as the basis for her TKOS.[2,3]

Fluo-4-measured Ca^{2+} imaging to assess calcium handling

iPSC-CMs cultured on 35-mm glass-bottom dishes (MatTek Corporation, Ashland, MA, USA) at 37°C, 5% CO_2 were loaded with 2 μM Fluo-4 AM (Thermo Fisher Scientific, Waltham, MA, USA) with 0.02% F-127 (Thermo Fisher Scientific, Waltham, MA, USA) in Tyrode's Solution (Alfa Aesar, Tewksbury, MA, USA) for 30 min. Following washout, Tyrode's solution was added, and cells were imaged. During imaging, cells were kept in a heated 37°C stage-top environment chamber supplied with 5% CO_2. Imaging of Ca^{2+} transients was taken under a 40× water objective using a Nikon Eclipse Ti (Melville, NY, USA) light microscope. iPSC-CMs were paced at 0.5 Hz using an IonOptix MyoPacer Field Stimulator (Westwood, MA, USA). Time-lapse videos were taken at a speed of 20 ms/frame for 20 s. For recordings with ISO, 1 μM ISO (I2760; MilliporeSigma) was added to the Tyrode's solution, and video recordings were taken between 6 and 10 min of incubation. The raw data were exported to Excel software (Microsoft, Redmond, WA, USA) and analyzed with a custom Excel-based script to correct for photo bleaching.

Electrophysiological LTCC measurement

Standard whole-cell patch-clamp technique was used to measure LTCC current at RT (22°C–24°C) with the use of an Axopatch 200B amplifier, Digidata 1440A and pClamp version 10.7 software (Molecular Devices, San Jose, CA, USA). The extracellular (bath) solution contained (mmol/L): 2 $CaCl_2$, 1 $MgCl_2$, 150 TEA-Cl, and 10 HEPES, pH adjusted to 7.35 with CsOH. For Ba^{2+} replacement measurements, we replaced $CaCl_2$ with 2 mmol/L $BaCl_2$. The intracellular (pipette) solution contained (mmol/L): 110 CsCl, 0.1 $CaCl_2$, 10 HEPES, 10 EGTA, 2 MgATP, and 10 TEA-Cl, pH adjusted to 7.30 with CsOH.[11] For low EGTA conditions, the concentration of EGTA in the intracellular solution was 0.2 mmol/L. Microelectrodes were pulled on a P-97 puller (Sutter Instruments, Novato, CA, USA) and fire polished to a final resistance of 2–3 MΩ. Series resistance was compensated by 80%–85%. Currents were filtered at 1 kHz and digitized at 5 kHz with an eight-pole Bessel filter. Data were analyzed using Clampfit (Axon Instruments, Sunnyvale, CA, USA) and Excel (Microsoft) and graphed with GraphPad Prism 8.3 (GraphPad Software, San Diego, CA, USA). The voltage dependence of activation curve was fitted with a Boltzmann function: G_{Ca}/G_{Ca} max = $\{1 + \exp[(V - V_{1/2})/k]\}^{-1}$, where $V_{1/2}$ and k are the half-maximal voltage of activation and the slope factor, respectively. The steady-state inactivation curve was fitted with a Boltzmann function: I_{Ca}/I_{Ca} max = $\{1 + \exp[(V - V_{1/2})/k]\}^{-1}$, where $V_{1/2}$ and k are the half-maximal voltage of inactivation and the slope factor, respectively. I_{Ca} decay was fitted with a biexponential function: $y = y_0 + \{1 - [A_f \exp(-t/\tau_f)] + [A_s \exp(-t/\tau_s)]\}$, where A_f and A_s represent the amplitudes of the fast and the slow inactivating components, respectively, and τ_f and τ_s represent the fast and slow time constants of inactivation, respectively. Persistent $Ca_V1.2$ current was measured at the end of a 500-ms-long depolarization of −20 mV.

Electrophysiological AP measurement

Whole-cell ruptured patch was used for AP recordings. APs were recorded at RT (22°C–24°C) using current-clamp mode at a constant rate of 1 Hz through 5-ms depolarizing current injections of 300–500 pA and gap-free configuration with the use of an Axopatch 200B amplifier, Digidata 1440A, and pClamp version 10.7 software. Following baseline measurement, 1 μM ISO was added to the bath solution, and APs were recorded again after 10-min incubation. The extracellular (bath) solution contained (mmol/L): 150 NaCl, 5.4 KCl, 1.8 CaCl2, 1 $MgCl_2$, 1 Na-pyruvate, and 15 HEPES, pH adjusted to 7.4 with NaOH. The pipette solution contained (mmol/L): 150 KCl, 5 NaCl, 2 $CaCl_2$, 5 EGTA, 5 MgATP, and 10 HEPES, pH adjusted to 7.2 with KOH. Data were analyzed using Clampfit, Excel (Microsoft) and graphed with GraphPad Prism 8.3 (GraphPad Software). Microelectrodes were pulled on a P-97 puller (Sutter Instruments) and fire polished to a final resistance of 2–3 MΩ. Series resistance was compensated by 80%–85%.

Arrhythmia events measurement

In the first, third, and fourth panels in Figure 3B, all AP recordings from each cell were evaluated to determine whether a particular arrhythmic event occurred in any of those recordings. Then the percentage of cells (both WT and $TRDN^{-/-}$) that exhibited a particular arrhythmic event was calculated by dividing the number of

cells with an arrhythmia by the total number of cells. Finally, a Fisher's exact test was used to determine whether there was a statistical difference between the number of WT and TRDN$^{-/-}$ cells showing an arrhythmia.

In the second panel in Figure 3B, the number of DADs per AP (DADs/episode) was evaluated only in spontaneous (gap-free) AP recordings for each cell to count the total number of APs in those recordings and the number of DADs present in those same recordings. Finally, the number of DADs was divided by the total number of APs to derive the number of DADs per AP for each cell. Two-way ANOVAs with multiple comparisons tests were used to determine statistical significance. Although the data in the first panel in Figure 3B are getting at the number of cells showing DADs, the purpose of the measurements in the second panel is to assess the rate at which those DADs occur.

Statistics

All data are expressed as mean ± standard error of the mean (SEM). Error bars represent SEM. For all experiments, except western blots, individual data points represent measurements from one iPSC-CM, and these were considered technical replicates. For experiments comparing two groups (i.e., isogenic control vs. TRDN$^{-/-}$), technical replicates were derived from multiple CM differentiations, which were considered biological replicates. Technical replicates were then grouped for statistical analysis. Individual data points shown for western blot quantification represent separate CM differentiations. For continuous data, unpaired Student's t tests or Mann-Whitney tests were performed to determine statistical significance between two groups, and Kruskal-Wallis tests with post hoc Dunn's multiple comparisons tests were used to determine statistical significance between three groups. Two-way ANOVAs with multiple comparisons tests were used to determine statistical significance for more than three groups. For categorical data, Fischer's exact tests were used to determine significance between two groups. A p value $<5.0 \times 10^{-2}$ was considered to be significant. All statistical analysis was carried out using GraphPad Prism 8.3.

SUPPLEMENTAL INFORMATION

Supplemental information can be found online at https://doi.org/10.1016/j.stemcr.2023.04.005.

AUTHOR CONTRIBUTIONS

Conceptualization, D.J.C., D.Y., L.W., C.S.J.K., D.J.T., B.C.K., and M.J.A.;methodology, D.J.C., D.Y., L.W., C.S.J.K., W.Z. and S.M.D.;formal analysis, D.J.C., D.Y., L.W., C.S.J.K., and W.Z.; inves-tigation, D.J.C., D.Y., L.W., C.S.J.K., and W.Z.; writing – originaldraft, D.J.C. and D.Y.; writing – review & editing, D.J.T., B.C.K, and M.J.A.; visualization, D.J.C, D.Y., and D.J.T.; supervision, I.M., B.C.K., and M.J.A.; project admisinsta-tion, D.J.C. and D.J.T.; funding acquisition, D.J.C., L.W., B.C.K., and M.J.A.

ACKNOWLEDGMENTS

The authors thank the two children with TKOS and their parents for enrolling in this IRB-approved research study, which enabled these new revelations about TKOS to emerge. Research reported in this publication was supported by the National Heart, Lung, and Blood Institute of the National Institutes of Health under award numbers F31HL149131 (to D.J.C.) and R35 HL144980 (to B.C.K.), Leducq Foundation grant 18CVD05 (to B.C.K. and L.W.), and the Mayo Clinic Windland Smith Rice Comprehensive Sudden Cardiac Death Program (to M.J.A.).

CONFLICT OF INTERESTS

M.J.A. is a consultant for Abbott, ARMGO Pharma, Boston Scientific, Daiichi Sankyo, Invitae, LQT Therapeutics, Medtronic, and UpToDate. M.J.A. and Mayo Clinic are involved in equity/royalty relationships with AliveCor and Anumana. These relationships are all modest, and none of these entities have contributed to this study in any manner.

Received: July 27, 2022
Revised: April 7, 2023
Accepted: April 11, 2023
Published: May 9, 2023

REFERENCES

Altmann, H.M., Tester, D.J., Will, M.L., Middha, S., Evans, J.M., Eckloff, B.W., and Ackerman, M.J. (2015). Homozygous/compound heterozygous triadin mutations associated with autosomal recessive long QT syndrome and pediatric sudden cardiac arrest: elucidation of triadin knockout syndrome. Circulation *131*, 2051–2060.

Bongianino, R., and Priori, S.G. (2015). Gene therapy to treat cardiac arrhythmias. Nat. Rev. Cardiol. *12*, 531–546.

Broendberg, A., Dait, C., Bjerre, J., Pedersen, L., Nielsen, J., Corydon, T., and Jensen, H. (2017). A novel Triadin variant causes a severe clinical CPVT phenotype in two young brothers. EP Europace *19*, 340. (Abstract).

Burridge, P.W., Matsa, E., Shukla, P., Lin, Z.C., Churko, J.M., Ebert, A.D., Lan, F., Diecke, S., Huber, B., Mordwinkin, N.M., et al. (2014). Chemically defined generation of human cardiomyocytes. Nat. Methods *11*, 855–860.

Cacheux, M., Fauconnier, J., Thireau, J., Osseni, A., Brocard, J., Roux-Buisson, N., Brocard, J., Fauré, J., Lacampagne, A., and Marty, I. (2020). Interplay between triadin and calsequestrin in the pathogenesis of CPVT in the mouse. Mol. Ther. *28*, 171–179.

Chopra, N., and Knollmann, B.C. (2013). Triadin regulates cardiac muscle couplon structure and microdomain Ca2+ signalling: a path towards ventricular arrhythmias. Cardiovasc. Res. *98*, 187–191.

Chopra, N., Yang, T., Asghari, P., Moore, E.D., Huke, S., Akin, B., Cattolica, R.A., Perez, C.F., Hlaing, T., Knollmann-Ritschel, B.E.C., et al. (2009). Ablation of triadin causes loss of cardiac Ca2+ release units, impaired excitation-contraction coupling, and cardiac arrhythmias. Proc. Natl. Acad. Sci. USA *106*, 7636–7641.

Clemens, D.J., Gray, B., Bagnall, R.D., Tester, D.J., Dotzler, S.M., Giudicessi, J.R., Matthews, E., Semsarian, C., Behr, E.R., and Ackerman, M.J. (2020a). Triadin knockout syndrome is absent in a multicenter molecular autopsy cohort of sudden infant death syndrome and sudden unexplained death in the young and is extremely rare in the general population. Circ. Genom. Precis. Med. *13*, e002731.

Clemens, D.J., Tester, D.J., Giudicessi, J.R., Bos, J.M., Rohatgi, R.K., Abrams, D.J., Balaji, S., Crotti, L., Faure, J., Napolitano, C., et al. (2019). International Triadin Knockout Syndrome Registry: the clinical phenotype and treatment outcomes of patients with triadin knockout syndrome. Circ. Genom. Precis. Med. *12*, e002419.

Clemens, D.J., Tester, D.J., Marty, I., and Ackerman, M.J. (2020b). Phenotype-guided whole genome analysis in a patient with genetically elusive long QT syndrome yields a novel TRDN-encoded triadin pathogenetic substrate for triadin knockout syndrome and reveals a novel primate-specific cardiac TRDN transcript. Heart Rhythm *17*, 1017–1024.

Lieu, D.K., Liu, J., Siu, C.W., McNerney, G.P., Tse, H.F., Abu-Khalil, A., Huser, T., and Li, R.A. (2009). Absence of transverse tubules contributes to non-uniform Ca2+ wavefronts in mouse and human embryonic stem cell–derived cardiomyocytes. Stem Cells Dev. *18*, 1493–1500.

Engel, A.G., Redhage, K.R., Tester, D.J., Ackerman, M.J., and Selcen, D. (2017). Congenital myopathy associated with the triadin knockout syndrome. Neurology *88*, 1153–1156.

Estes, S.I., Ye, D., Zhou, W., Dotzler, S.M., Tester, D.J., Bos, J.M., Kim, C.S.J., and Ackerman, M.J. (2019). Characterization of the CACNA1C-R518C missense mutation in the pathobiology of long-QT syndrome using human induced pluripotent stem cell cardiomyocytes shows action potential prolongation and L-type calcium channel perturbation. Circ. Genom. Precis. Med. *12*, e002534.

Guo, W., and Campbell, K.P. (1995). Association of triadin with the ryanodine receptor and calsequestrin in the lumen of the sarcoplasmic reticulum. J. Biol. Chem. *270*, 9027–9030.

Guo, W., Jorgensen, A.O., Jones, L.R., and Campbell, K.P. (1996). Biochemical characterization and molecular cloning of cardiac triadin. J. Biol. Chem. *271*, 458–465.

Itzhaki, I., Maizels, L., Huber, I., Gepstein, A., Arbel, G., Caspi, O., Miller, L., Belhassen, B., Nof, E., Glikson, M., and Gepstein, L. (2012). Modeling of catecholaminergic polymorphic ventricular tachycardia with patient-specific human-induced pluripotent stem cells. J. Am. Coll. Cardiol. *60*, 990–1000.

Itzhaki, I., Maizels, L., Huber, I., Zwi-Dantsis, L., Caspi, O., Winterstern, A., Feldman, O., Gepstein, A., Arbel, G., Hammerman, H., et al. (2011). Modelling the long QT syndrome with induced pluripotent stem cells. Nature *471*, 225–229.

Knollmann, B.C. (2009). New roles of calsequestrin and triadin in cardiac muscle. J. Physiol. *587*, 3081–3087.

Kobayashi, Y.M., Alseikhan, B.A., and Jones, L.R. (2000). Localization and characterization of the calsequestrin-binding domain of triadin 1. Evidence for a charged beta-strand in mediating the protein-protein interaction. J. Biol. Chem. *275*, 17639–17646.

Lahat, H., Pras, E., Olender, T., Avidan, N., Ben-Asher, E., Man, O., Levy-Nissenbaum, E., Khoury, A., Lorber, A., Goldman, B., et al. (2001). A missense mutation in a highly conserved region of CASQ2 is associated with autosomal recessive catecholamine-induced polymorphic ventricular tachycardia in Bedouin families from Israel. Am. J. Hum. Genet. *69*, 1378–1384.

Maguy, A., Kucera, J.P., Wepfer, J.P., Forest, V., Charpentier, F., and Li, J. (2020). KCNQ1 antibodies for immunotherapy of long QT syndrome type 2. J. Am. Coll. Cardiol. *75*, 2140–2152.

Marty, I. (2015). Triadin regulation of the ryanodine receptor complex. J. Physiol. *593*, 3261–3266.

O'Callaghan, B.M., Hancox, J.C., Stuart, A.G., Armstrong, C., Williams, M.M., Hills, A., Pearce, H., Dent, C.L., Gable, M., and Walsh, M.A. (2018). A unique triadin exon deletion causing a null phenotype. HeartRhythm Case Rep. *4*, 514–518.

Oddoux, S., Brocard, J., Schweitzer, A., Szentesi, P., Giannesini, B., Brocard, J., Fauré, J., Pernet-Gallay, K., Bendahan, D., Lunardi, J., et al. (2009). Triadin deletion induces impaired skeletal muscle function. J. Biol. Chem. *284*, 34918–34929.

Ran, F.A., Hsu, P.D., Wright, J., Agarwala, V., Scott, D.A., and Zhang, F. (2013). Genome engineering using the CRISPR-Cas9 system. Nat. Protoc. *8*, 2281–2308.

Rizzi, N., Liu, N., Napolitano, C., Nori, A., Turcato, F., Colombi, B., Bicciato, S., Arcelli, D., Spedito, A., Scelsi, M., et al. (2008). Unexpected structural and functional consequences of the R33Q homozygous mutation in cardiac calsequestrin. Circ. Res. *103*, 298–306.

Rooryck, C., Kyndt, F., Bozon, D., Roux-Buisson, N., Sacher, F., Probst, V., and Thambo, J.-B. (2015). New family with catecholaminergic polymorphic ventricular tachycardia linked to the triadin gene. J. Cardiovasc. Electrophysiol. *26*, 1146–1150.

Rossi, D., Gigli, L., Gamberucci, A., Bordoni, R., Pietrelli, A., Lorenzini, S., Pierantozzi, E., Peretto, G., De Bellis, G., Della Bella, P., et al. (2019). A novel homozygous mutation in the *TRDN* gene causes a severe form of pediatric malignant ventricular arrhythmia. Heart Rhythm *17*, 296–304.

Roux-Buisson, N., Cacheux, M., Fourest-Lieuvin, A., Fauconnier, J., Brocard, J., Denjoy, I., Durand, P., Guicheney, P., Kyndt, F., Leenhardt, A., et al. (2012). Absence of triadin, a protein of the calcium release complex, is responsible for cardiac arrhythmia with sudden death in human. Hum. Mol. Genet. *21*, 2759–2767.

Schwartz, P.J., Ackerman, M.J., Antzelevitch, C., Bezzina, C.R., Borggrefe, M., Cuneo, B.F., and Wilde, A.A.M. (2020). Inherited cardiac arrhythmias. Nat. Rev. Dis. Primers *6*, 58.

Sleiman, N.H., McFarland, T.P., Jones, L.R., and Cala, S.E. (2015). Transitions of protein traffic from cardiac ER to junctional SR. J. Mol. Cell. Cardiol. *81*, 34–45.

Walsh, M.A., Stuart, A.G., Schlecht, H.B., James, A.F., Hancox, J.C., and Newbury-Ecob, R.A. (2016). Compound heterozygous triadin mutation causing cardiac arrest in two siblings. Pacing Clin. Electrophysiol. *39*, 497–501.

Wang, L., Kim, K., Parikh, S., Cadar, A.G., Bersell, K.R., He, H., Pinto, J.R., Kryshtal, D.O., and Knollmann, B.C. (2018). Hypertrophic cardiomyopathy-linked mutation in troponin T causes myofibrillar disarray and pro-arrhythmic action potential changes in human iPSC cardiomyocytes. J. Mol. Cell. Cardiol. *114*, 320–327.